Comparison between closure phase and phase referenced interferometric image reconstructions

Nuno Gomes[a, b, c], Paulo J. V. Garcia[c, d], Eric Thiébaut[e], Stéphanie Renard[d], Mercedes Filho[f]

[a]European Organisation for Astronomical Research in the Southern Hemisphere (ESO), Karl-Schwarzschild-Straße 2, Garching bei München, D-85748 München, Germany;
[b]Faculdade de Ciências da Universidade do Porto (FCUP), Rua do Campo Alegre, s/n, 4169-007 Porto, Portugal;
[c]Laboratório de Sistemas, Instrumentação e Modelação em Ciências e Tecnologias do Ambiente e do Espaço (SIM)/Faculdade de Engenharia da Universidade do Porto (FEUP), Rua Dr. Roberto Frias, s/n, 4200-465 Porto, Portugal;
[d]Laboratoire d'Astrophysique, Observatoire de Grenoble (LAOG), 414, Rue de la Piscine, Saint-Martin d'Héres, France;
[e]Centre de Recherche Astrophysique de Lyon (CRAL)/Observatoire de Lyon, 9, Avenue Charles André, 69561 Saint-Genis Laval Cédex, France;
[f]Centro de Astrofísica da Universidade do Porto (CAUP), Rua das Estrelas, 4150-762 Porto, Portugal;

ABSTRACT

We compare the quality of interferometric image reconstructions for two different sets of data: square of the visibility plus closure phase (e.g. AMBER like case) and square of the visibility plus visibility phase (e.g. PRIMA+AMBER or GRAVITY like cases). We used the Multi-aperture image Reconstruction Algorithm for reconstructions of test cases under different signal-to-noise ratios and noisy data (squared visibilities and phases). Our study takes into account noise models based on the statistics of visibility, phase and closure phase. We incorporate the works developed by Tatulli and Chelly (2005) on the noise of the power-spectrum and closure phase in the read-out and photon noise regimes,[1] and by Colavita (1999) on the signal-to-noise ratio of the visibility phase.[2] The final images were then compared to the original one by means of positions and fluxes, computing the astrometry and the photometry. For the astrometry, the precision was typically of tens of microarcseconds, while for the photometry, it was typically of a few percent. Although both cases are suitable for image restorations of real interferometric observations, the results indicate a better performance of phase referencing (V^2 + visibility phase) in a low signal-to-noise ratio scenario.

Keywords: Interferometry, PRIMA, power-spectrum, visibility phase, phase referencing, closure phase, imaging, MiRA

1. INTRODUCTION

Image reconstruction is a key problem in optical interferometry. Data is obtained in a sparse coverage of the Fourier plane (UV plane), not in the form of an image. By means of visibility and closure phase information and supported by physical models, modern optical interferometers allow one to yield reconstructed images of real objects.[3,4] The Phase-Referenced Imaging and Micro-arcsecond Astrometry (PRIMA) dual-feed facility, recently installed at the Very Large Telescope Interferometer (VLTI), will offer a phase referenced imaging mode, where data consisting on spectrally dispersed visibilities and phases can be used to generate images.[5,6] The second generation instrument General Relativity Analysis via VLT InterferometrY (GRAVITY),[7] to be implemented in the VLTI during this decade, will use four telescopes simultaneously in order to achieve an accuracy of 10 μas in astrometry on six baselines and to offer phase referencing on faint targets (K $\geq$ 15).[8] Therefore, two

Further author information: send correspondence to Nuno Gomes. E-mail: ngomes@eso.org.

scenarios for interferometric image reconstruction arise from current facilities: power-spectrum + closure phase data (hereafter referred as *closure phase* case) and power-spectrum + visibility phase data (hereafter referred as *phase referencing* case).

During the last decade, tests have been done to study the behaviour of reconstruction algorithms using synthetic images and different sets of data.[9–13] However, the used noise models did not always correspond to real situations, although efforts were developed in order to produce data as similar to real interferometric data as possible.[9–11] Filho et al. (2008) estimated the uncertainties on squared visibilities, phases and closure phases assuming an interferometer able of multi-axial recombinations with a fringe tracker.[12,13] We used the work by Colavita (1999) to estimate the uncertainties in the phase[2] and the models developed by Tatulli and Chelli (2005)[1] to estimate the statistics of the power-spectrum and closure phase.

We devised a simple method (described in detail in the following sections) to perform a formal comparison between images belonging to both cases. A synthetic image of a cluster of eight stars was built. The cluster was used to create several Optical Interferometry FITS exchange format (OIFITS) files, each corresponding to a different set of signal-to-noise ratios (SNRs) and noisy data. All files were used as input to the Multi-aperture image Reconstruction Algorithm (MiRA).[14] A set of optimal parameters (initial guess, number of steps and regularisation) was found and kept for all the restorations, allowing one to compare the resulting images under the same conditions. Using `Starfinder`[15] and `SExtractor`,[16] the astrometry and the photometry of the images were measured. We computed the distances and the relative fluxes between each element of the cluster and the brightest star. These data were used to evaluate the quality of the reconstructions and to compare the images with the original one.

2. SETUP

The cluster corresponds to eight stars with a Gaussian intensity profile. The amplitudes of the Gaussians decrease by a factor of 2, having the brightest an unity amplitude and the faintest the value 1/128. The width of the Gaussian σ is 0.5 mas for all the stars. The cluster is approximately 22.4 mas (140 pixels) wide and the field of view (FOV) of the image corresponds to a square of 80 mas width (500 pixels). The cluster and the plot of the uv-coverage can be seen in Figure 1.

The image was used to build standard OIFITS files, using the VLTI as a template: 6 Auxiliary Telescopes (ATs) occupying stations A0-B1-D2-G1-J2-M0, object located at a $-60°$ declination angle, entire transit of 9 hours, uv-integration time of 1 hour and a central wavelength of 2.2 μm. The set-up was chosen in order to optimize the uv-coverage.

Regarding the SNR, which in our simulations is controlled by the total number of photons N reaching the array of telescopes, three scenarios were considered: $N \sim 10^7$, $N \sim 10^5$ and $N \sim 10^3$ photons. The errors for the power-spectrum and closure phase, in photon and detector regimes, were based on the work developed by Tatulli and Chelli (2005).[1] For the absolute phase, the errors were calculated according to the model of Colavita (1999).[2] For the power-spectrum, the detector noise regime is considered ($N \ll 1$), while for the closure phase, both the photon ($N \gg 1$) and detector noise regimes are taken in to account. Some approximations were implemented: Strehl equal to 1 and Strehl error equal to 0, transmission in the optical fibre equal to 1 and the fraction of light selected for photometry at the output of the beam splitter was neglected. All errors were randomly added to the data by means of a uniform distribution. For each group of three realisations corresponding to a specific N, we computed the mean of the medians of the SNR of the power-spectrum (V^2), phase (ϕ) and closure phase (ϕ_3) – see Table 1.

3. IMAGE RESTORATIONS

For each SNR scenario, three OIFITS were generated and used as input to MiRA algorithm, in order to restore an image. Both for *closure phase* and *phase referencing* cases, MiRA was configured under a positivity constraint, using a *quadratic* or *edge-preserving smoothness* regularisation, a normalised image of 500 × 500 pixels (100 × 100 mas) and pixel size equal to 0.20 mas. We used $\lambda = 2.2$ μm for the simulation. The choice of a smooth regularisation is justified by the fact that the cluster does not present any high frequency contents due to point-like sources or sharp edges.[14] We selected a FOV big enough (at least three times larger than the object of

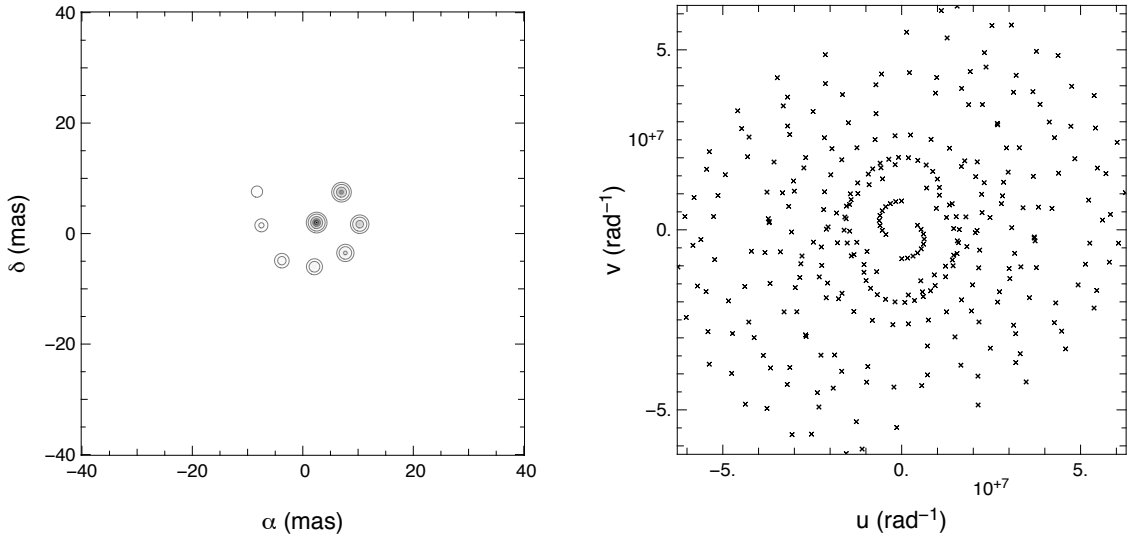

(a) The cluster is approximately 22.4 mas wide and is embedded in a FOV of 80 mas × 80 mas (500×500 pixels); the pixel size is approximately equal to 0.16 mas. The contour levels are at 1, 10, 40 and 90%.

(b) *uv*-coverage corresponding to a 6 ATs configuration (A0-B1-D2-G1-J2-M0), not available in VLTI yet.

Figure 1. Contour plot of the synthetic cluster of stars used as a model for the reconstructions (a) and *uv*-coverage with the VLTI interferometer (b).

Table 1. Mean of the medians of the SNRs of the power-spectrum (V^2), phase (ϕ) and closure phase (ϕ_3).

	$N \sim 10^7$	$N \sim 10^5$	$N \sim 10^3$
V^2	396.25	39.69	3.93
ϕ	875.0	87.7	9
ϕ_3	3	1	1

interest) as means to get the cluster concentrated in the centre of the image. This is necessary when using fast Fourier transforms (FFTs) in MiRA, otherwise the algorithm does not produce reconstructed images with good quality.* Figures 2, 3 and 4 represent grids with all the reconstructed images.

Using `SExtractor`[16] (and `Starfinder`[15] as a verification), the restored stars were detected and their relative coordinates and fluxes determined. The thresholds were selected in a way that allowed `SExtractor` and `Starfinder` to find at least all the reconstructed stars of the cluster. The correct stars were then selected by plotting the found sources over the reconstructed images. For every image, using the astrometry, the distances between every star and the brightest one were calculated. Using the photometry, the ratio of the fluxes between each star of the cluster and the brightest one in the corresponding image were also computed. The distances, fluxes and ratios of the latter were compared with the values in the synthetic reference image and the absolute errors calculated. The results are compiled in Tables 2 through 13 (see end of document).

4. RESULTS

In the case of the best SNR, all stars were reconstructed and almost any spur structures were created by the algorithm in both *closure phase* and *phase referencing* cases, although the images reconstructed with square of the amplitude + closure phase data were cleaner than the ones with square of the amplitude + phase data. Moreover, the shape of the stars in the former case was very close to the circular (true) one, while this was not

*This care is not necessary when using exact Fourier transforms (EFTs).

the case for the latter, specially for the fainter stars – see Figure 2. The distances, fluxes and flux ratios are in excellent agreement with the reference values in both cases – see Tables 2–5.

For the scenario of intermediate value of SNR, the faintest star was not always restored, specially in the *closure phase* case. In the first reconstructed image of this case, several artefacts appeared in the field and the brightness of some of those structures was of the order of magnitude of the flux of the two faintest stars (the faintest star was not restored). In the *phase referencing* case, only in one image the faintest star was missing. The shape of the objects was approximately circular and all the images were clean of artefacts – see Figure 3. The distances, fluxes and flux ratios are in good agreement with the reference values in both cases, although the errors of the flux of the two faintest stars are of the same order of magnitude than the flux itself – see Tables 6–9.

In the last (worst) SNR scenario, the results are quite different for the two cases under study. *Closure phase* case presents a plethora of spur features spread in the FOV. Only four or five stars were reconstructed and, except for the brightest one, their shapes were elongated. Although many false structures were also created in the *phase referencing* case and the shapes of the stars were similarly elongated, the background noise was smaller and there were more stars restored (at least six) – see Figure 4. The distances of the reconstructed stars are in excellent agreement with the reference values, but only in the *phase referencing* case the fluxes well agree with the reference values for all the stars – see Tables 10–13.

5. ANALYSIS AND CONCLUSIONS

One of the main problems of image reconstruction is the calibration of the visibilities. In our work, we have been considering stochastic errors, but calibration errors, which change between observation nights, might dominate the uncertainties. In that perspective, this simulation is not realistic.

Since the holes in the *uv*-plane yield spur and unreal structures during the image reconstruction process, especially if the SNR is low, we compared the reconstructed images with the synthetic one. In the absence of the true image, the identification of real sources and artefacts would be possible computing the dynamic range of the reconstructed image. As it is denoted by the astrometry and photometry of the individual stars, broadly speaking, MiRA fared well with the image reconstructions of the cluster using both sets of data (*power-spectra + closure phases* and *power-spectra + visibility phases*). Under the imposed conditions, it was able to fairly reconstruct the first five stars. Their relative positions are correct, their shapes are well reproduced and most of the flux is restored. The flux ratio between those stars corresponds to a difference of 3 magnitudes. Considering the phase referencing case, at least six stars were restored, which corresponds to a magnitude difference of nearly 4. Only for the faintest stars, with fluxes less than 4% of the brightest star, the reconstruction is of inferior quality: in the lower SNR scenarios, their positions and fluxes are not well determined and, sometimes, they are not even restored at all. Subsequent tests developed by us indicate that better precisions are achieved when using exact Fourier transforms in MiRA. More profound and individually tuned reconstruction processes could lead to the restoration of all the stars in the three SNR scenarios, but we decided to keep the same relatively simple process for all the cases with the purpose of performing unbiased comparisons between them.

The results seem to indicate that when using FFTs in MiRA, the *phase referencing* case gives better results than the *closure phase* case in a low SNR scenario. This is not surprising, as more information about the *uv*-plane is available in the first case. Moreover, since typically the closure phase is smaller than the visibility phase and the noise of the former is larger than the noise of the latter, the SNR on the closure phase is smaller.

ACKNOWLEDGMENTS

This research is partially supported by Fundação para a Ciência e Tecnologia Ph.D. grants SFRH/BD/44282/2008 and PTDC/CTE-AST/098034/2008. The authors want to thank Patrícia Figueiró Spinelli and André Müller for their valuable help in using `SExtractor` and `Starfinder`, respectively. All calculations, graphics and images were performed and created with `Yorick` (`http://yorick.sourceforge.net`), which is available for free.

REFERENCES

[1] Tatulli, E. and Chelli, A., "Fiber optic interferometry: statistics of visibility and closure phase," *Optical Society of America Journal* **22**(8), 1589–1599 (2005).

[2] Colavita, M. M., Wallace, J. K., Hines, B. E., Gursel, Y., Malbet, F., Palmer, D. L., Pan, X. P., Shao, M., Yu, J. W., Boden, A. F., Dumont, P. J., Gubler, J., Koresko, C. D., Kulkarni, S. R., Lane, B. F., Mobley, D. W., and van Belle, G. T., "The Palomar Testbed Interferometer," *The Astrophysical Journal* **510**(1), 505–521 (1999).

[3] Haubois, X., Perrin, G., Lacour, S., Verhoelst, T., Meimon, S. C., Mugnier, L., Thiébaut, E., Berger, J.-P., Ridgway, S. T., Monnier, J. D., Millan-Gabet, R., and Traub, W. A., "Imaging the spotty surface of Betelgeuse in the H band," *Astronomy & Astrophysics* **508**, 923–932 (2009).

[4] Lacour, S., Thiébaut, E., Perrin, G., Meimon, S. C., Haubois, X., Pedretti, E., Ridgway, S. T., Monnier, J. D., Berger, J.-P., Schuller, P. A., Woodruff, H., Poncelet, A., Le Coroller, H., and Millan-Gabet, R., "The Pulsation of Chi Cygni Imaged by Optical Interferometry: a Novel Technique to Derive Distance and Mass of Mira Stars," *The Astrophysical Journal* **707**, 632–643 (2009).

[5] Delplancke, F., Derie, F., Paresce, F., Glindemann, A., Lévy, F., Lévêque, S., and Ménardi, S., "Prima for the VLTI Science," *Astrophysics and Space Science* **286**, 99–104 (2003).

[6] Delplancke, F., "The PRIMA facility phase-referenced imaging and micro-arcsecond astrometry," *New Astronomy Reviews* **52**, 199–207 (2008).

[7] Eisenhauer, F., Perrin, G., Brandner, W., Straubmeier, C., Richichi, A., Gillessen, S., Berger, J.-P., Hippler, S., Eckart, A., Schöller, M., Rabien, S., Cassaing, F., Lenzen, R., Thiel, M., Clénet, Y., Ramos, J. R., Kellner, S., Fédou, P., Baumeister, H., Hofmann, R., Gendron, E., Boehm, A., Bartko, H., Haubois, X., Klein, R., Dodds-Eden, K., Houairi, K., Hormuth, F., Gräter, A., Jocou, L., Naranjo, V., Genzel, R., Kervella, P., Henning, T., Hamaus, N., Lacour, S., Neumann, U., Haug, M., Malbet, F., Laun, W., Kolmeder, J., Paumard, T., Rohloff, R.-R., Pfuhl, O., Perraut, K., Ziegleder, J., Rouan, D., and Rousset, G., "GRAVITY: getting to the event horizon of Sgr A*," in [*Optical and Infrared Interferometry*], Schöller, M., Danchi, W. C., and Delplancke, F., eds., 70132A–70132A–13, SPIE Astronomical Instrumentation, Marseille, France (2008).

[8] van Belle, G. T., Sahlmann, J., Abuter, R., Accardo, M., Andolfato, L., Brillant, S., de Jong, J., Derie, F., Delplancke, F., Duc, T. P., Dupuy, C., Gilli, B., Gitton, P., Haguenauer, P., Jocou, L., Jost, A., Di Lieto, N., Frahm, R., Ménardi, S., Morel, S., Moresmau, J.-M., Palsa, R., Popovic, D., Pozna, E., Puech, F., Lévêque, S., Ramirez, A., Schuhler, N., Somboli, F., Wehner, S., and Consortium, E., "The VLTI PRIMA Facility," *The Messenger* **134**(December), 6–11 (2008).

[9] Lawson, P. R., Cotton, W. D., Hummel, C. A., Monnier, J. D., Zhao, M., Young, J. S., Thorsteinsson, H., Meimon, S. C., Mugnier, L., Le Besnerais, G., Thiébaut, E., and Tuthill, P. G., "An interferometry imaging beauty contest," in [*New Frontiers in Stellar Interferometry*], Wesley, A. and Bellingham, T., eds., **5491**, SPIE (2004).

[10] Lawson, P. R., Cotton, W. D., Hummel, C. A., Baron, F., Young, J. S., Kraus, S., Hofmann, K.-H., Weigelt, G. P., Ireland, M., Monnier, J. D., Thiébaut, E., Rengaswamy, S., and Chesneau, O., "2006 Interferometry Imaging Beauty Contest," in [*Advances in Stellar Interferometry*], Monnier, J. D., Schöller, M., and Danchi, W. C., eds., **6268**(818), 1–12, SPIE (2006).

[11] Cotton, W. D., Monnier, J. D., Baron, F., Hofmann, K.-H., Kraus, S., Weigelt, G. P., Rengaswamy, S., Thiébaut, E., Lawson, P. R., Jaffe, W., Hummel, C. A., Pauls, T. A., Schmitt, H., Tuthill, P. G., and Young, J. S., "2008 Imaging Beauty Contest," in [*Optical and Infrared Interferometry*], Schöller, M., Danchi, W. C., and Delplancke, F., eds., **7013**, 70131N–70131N–14, SPIE (2008).

[12] Filho, M. E., Renard, S., Garcia, P. J. V., Duvert, G., Duchêne, G., Thiébaut, E., Young, J. S., Absil, O., Berger, J.-P., Beckert, T., Hoenig, S., Schertl, D., Weigelt, G. P., Testi, L., Tatulli, E., Borkowski, V., de Becker, M., Surdej, J., Aringer, B., Hron, J., Lebzelter, T., Chiavassa, A., Corradi, R., and Harries, T. J., "Phase Closure Image Reconstruction for Future VLTI Instrumentation," in [*Optical and Infrared Interferometry*], Schöller, M., Danchi, W. C., and Delplancke, F., eds., **7013**(2008), 70133Z–70133Z–10, SPIE (2008).

[13] Filho, M. E., Garcia, P. J. V., Duvert, G., Duchene, G., Thiébaut, E., Young, J. S., Absil, O., Berger, J.-P., Beckert, T., Hoenig, S., Schertl, D., Weigelt, G., Testi, L., Tatulli, E., Borkowski, V., de Becker, M., Surdej, J., Aringer, B., Hron, J., Lebzelter, T., Chiavassa, A., Corradi, R., and Harries, T. J., "Phase Referencing in Optical Interferometry," in [*Optical and Infrared Interferometry*], Schöller, M., Danchi, W. C., and Delplancke, F., eds., 70131F–70131F–12 (2008).

[14] Thiébaut, E., "MIRA: an effective imaging algorithm for optical interferometry," in [*Optical and Infrared Interferometry*], Schöller, M., Danchi, W. C., and Delplancke, F., eds., **7013**(3), 70131I–70131I–12, SPIE (2008).

[15] Diolaiti, E., Bendinelli, O., Bonaccini, D., Close, L. M., Currie, D. G., and Parmeggiani, G., "StarFinder: an IDL GUI based code to analyze crowded fields with isoplanatic correcting PSF fitting," in [*Adaptive Optical Systems Technology*], Wizinowich, P. L., ed., 879–888, SPIE (2000).

[16] Bertin, E. and Arnouts, S., "SExtractor: Software for source extraction," *Astronomy and Astrophysics Supplement* **117**, 393–404 (1996).

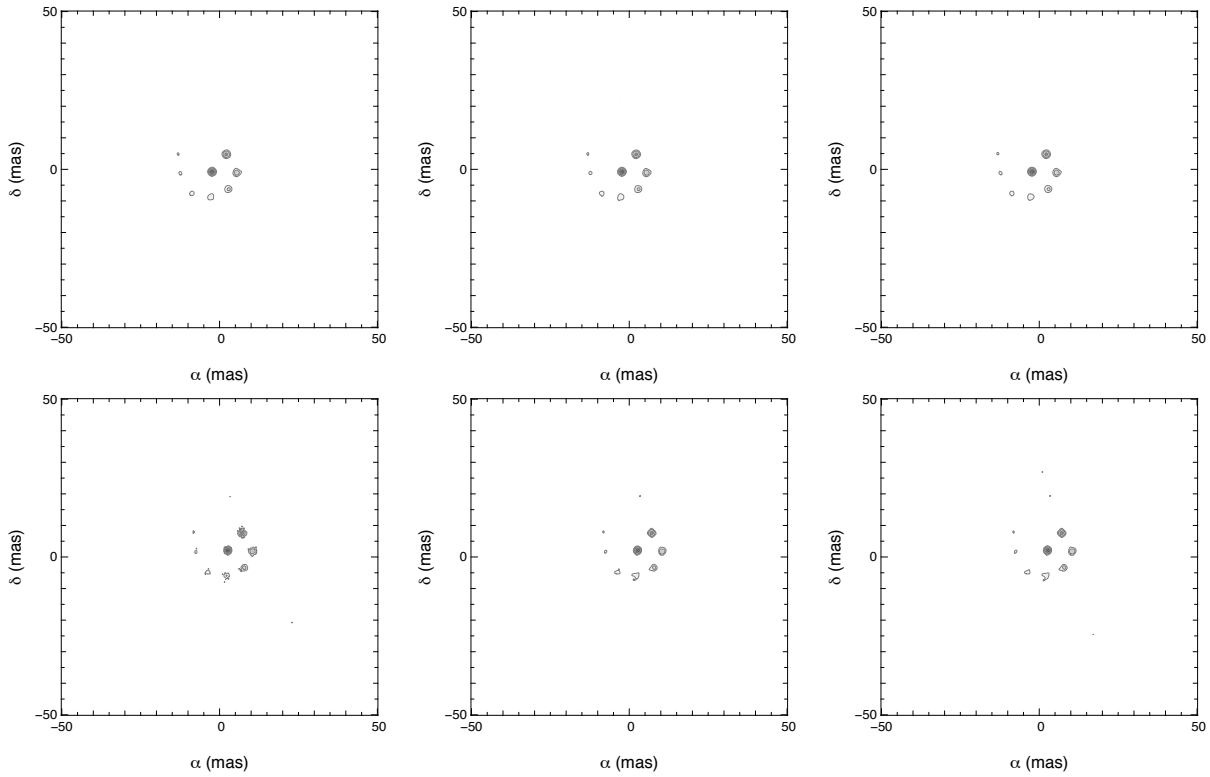

Figure 2. Contour plots of the reconstructed images for the $N \sim 10^7$ scenario. *Top row*: *closure phase* case; *bottom row*: *phase referencing* case. The contour levels are at 1, 10, 40 and 90%.

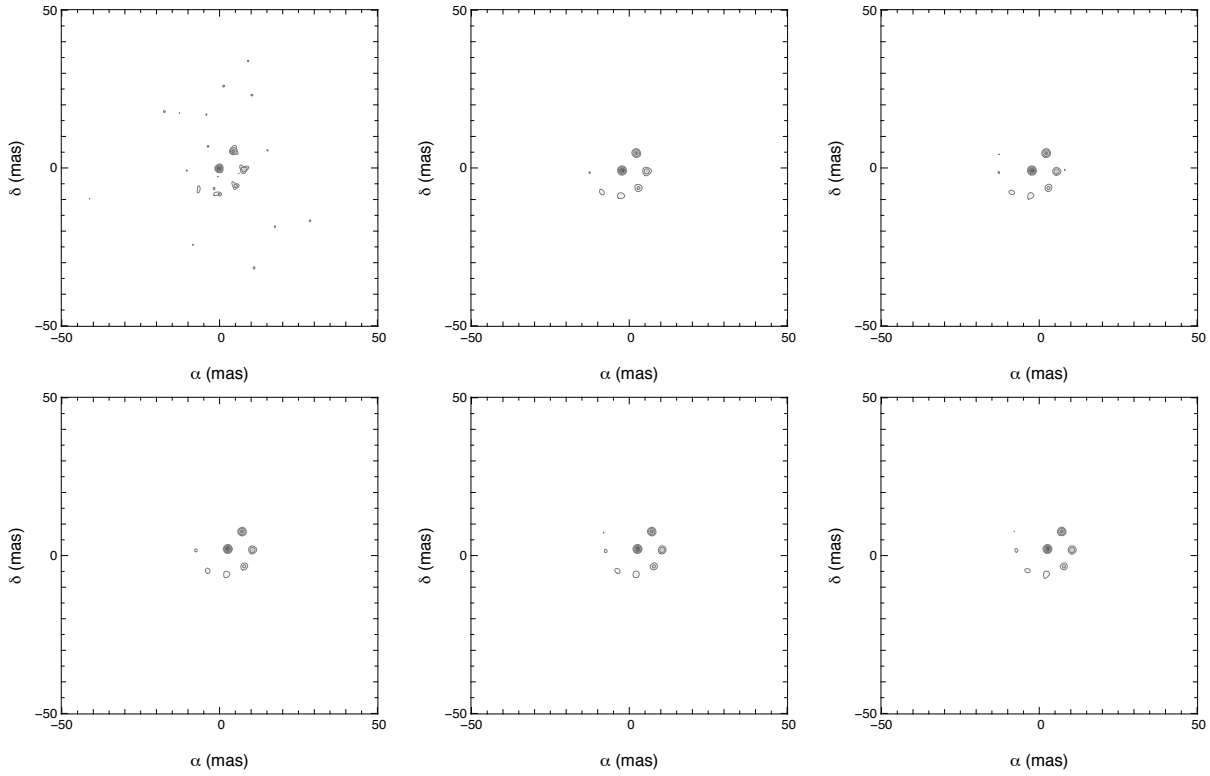

Figure 3. Contour plots of the reconstructed images for the $N \sim 10^5$ scenario. *Top row*: *closure phase* case. *Bottom row*: *phase referencing* case. The contour levels are at 1, 10, 40 and 90%.

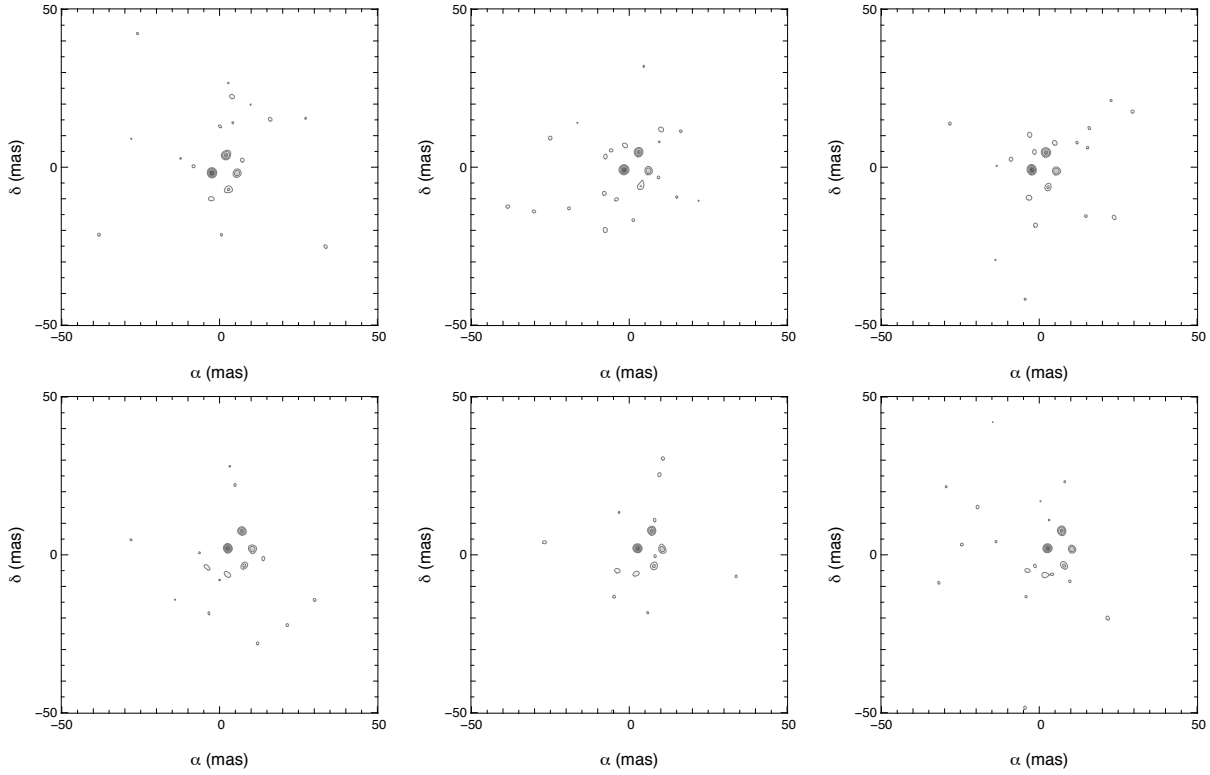

Figure 4. Contour plots of the reconstructed images of the $N \sim 10^3$ scenario. *Top row*: *closure phase* case; *bottom row*: *phase referencing* case. The contour levels are at 1, 10, 40 and 90%.

Table 2. Astrometry of the reference and first set ($N \sim 10^7$) of reconstructed images using closure phase information. The "*Reference*" column refer to the synthetic image. The distances are in respect to the brightest star.

Star No.	**Reference Distance** (mas)	**Distance** (mas)
2	7.11	7.12 ± 0.02
3	7.81	7.83 ± 0.02
4	7.57	7.58 ± 0.02
5	8.010	8.019 ± 0.009
6	9.34	9.39 ± 0.05
7	10.012	10.007 ± 0.006
8	12.166	12.174 ± 0.009

Table 3. Photometry of the reference and first set ($N \sim 10^7$) of reconstructed images using closure phase information. The "*Reference*" column refer to the synthetic image. The flux ratios are in respect to the brightest star.

Star No.	**Reference Flux** (relative)	**Flux** (relative)	**Reference Flux Ratio**	**Flux Ratio**
1	0.5008	$(5.013 \pm 0.004) \times 10^{-1}$	–	–
2	0.250	$(2.54 \pm 0.03) \times 10^{-1}$	0.50000	$(5.0616 \pm 0.0006) \times 10^{-1}$
3	0.1252	$(1.255 \pm 0.002) \times 10^{-1}$	0.249989	$(2.50270 \pm 0.00003) \times 10^{-1}$
4	0.063	$(6.1 \pm 0.1) \times 10^{-2}$	0.12502	$(1.2553 \pm 0.0002) \times 10^{-1}$
5	0.0313	$(3.05 \pm 0.08) \times 10^{-2}$	0.06249	$(6.087 \pm 0.002) \times 10^{-2}$
6	0.016	$(1.4 \pm 0.2) \times 10^{-2}$	0.03125	$(2.716 \pm 0.004) \times 10^{-2}$
7	0.008	$(6 \pm 2) \times 10^{-3}$	0.01562	$(1.113 \pm 0.004) \times 10^{-2}$
8	0.004	$(2 \pm 2) \times 10^{-3}$	0.00781	$(4.73 \pm 0.03) \times 10^{-3}$

Table 4. Astrometry of the reference and first set ($N \sim 10^7$) of reconstructed images using visibility phase information. The "*Reference*" column refer to the synthetic image. The distances are in respect to the brightest star.

Star No.	**Reference Distance** (mas)	**Distance** (mas)
2	7.11	7.12 ± 0.02
3	7.81	7.83 ± 0.02
4	7.569	7.574 ± 0.005
5	8.010	8.018 ± 0.008
6	9.34	9.39 ± 0.05
7	10.01	10.10 ± 0.09
8	12.2	12.3 ± 0.1

Table 5. Photometry of the reference and first set ($N \sim 10^7$) of reconstructed images using visibility phase information. The "*Reference*" column refer to the synthetic image. The flux ratios are in respect to the brightest star.

Star No.	**Reference Flux** (relative)	**Flux** (relative)	**Reference Flux Ratio**	**Flux Ratio**
1	0.5008	$(5.007 \pm 0.002) \times 10^{-1}$	–	–
2	0.250	$(2.56 \pm 0.06) \times 10^{-1}$	0.5000	$(5.121 \pm 0.001) \times 10^{-1}$
3	0.125	$(1.27 \pm 0.02) \times 10^{-1}$	0.24999	$(2.5430 \pm 0.0004) \times 10^{-1}$
4	0.063	$(6.1 \pm 0.2) \times 10^{-2}$	0.12502	$(1.2128 \pm 0.0004) \times 10^{-1}$
5	0.031	$(3.0 \pm 0.02) \times 10^{-2}$	0.06249	$(5.943 \pm 0.003) \times 10^{-2}$
6	0.016	$(1.4 \pm 0.2) \times 10^{-2}$	0.03125	$(2.792 \pm 0.003) \times 10^{-2}$
7	0.008	$(5 \pm 3) \times 10^{-3}$	0.0156	$(9.77 \pm 0.06) \times 10^{-3}$
8	0.004	$(2 \pm 2) \times 10^{-3}$	0.00781	$(3.12 \pm 0.05) \times 10^{-3}$

Table 6. Astrometry of the reference and second set ($N \sim 10^5$) of reconstructed images using closure phase information. The "*Reference*" column refer to the synthetic image. The distances are in respect to the brightest star.

Star No.	**Reference Distance** (mas)	**Distance** (mas)
2	7.11	7.13 ± 0.02
3	7.81	7.83 ± 0.02
4	7.57	7.59 ± 0.02
5	8.01	8.00 ± 0.01
6	9.3	9.4 ± 0.1
7	10.0	10.3 ± 0.3
8	12.2	11.6 ± 0.5

Table 7. Photometry of the reference and second set ($N \sim 10^5$) of reconstructed images using closure phase information. The "*Reference*" column refer to the synthetic image. The flux ratios are in respect to the brightest star.

Star No.	**Reference Flux** (relative)	**Flux** (relative)	**Reference Flux Ratio**	**Flux Ratio**
1	0.501	$(5.04 \pm 0.03) \times 10^{-1}$	–	–
2	0.250	$(2.53 \pm 0.03) \times 10^{-1}$	0.50000	$(5.0336 \pm 0.0003) \times 10^{-1}$
3	0.125	$(1.26 \pm 0.01) \times 10^{-1}$	0.249989	$(2.50713 \pm 0.00007) \times 10^{-1}$
4	0.063	$(5.8 \pm 0.4) \times 10^{-2}$	0.12502	$(1.1570 \pm 0.0009) \times 10^{-1}$
5	0.031	$(2.9 \pm 0.3) \times 10^{-2}$	0.06249	$(5.661 \pm 0.006) \times 10^{-2}$
6	0.016	$(1.3 \pm 0.3) \times 10^{-2}$	0.03125	$(2.490 \pm 0.006) \times 10^{-2}$
7	0.008	$(2 \pm 5) \times 10^{-3}$	0.016	$(4.8 \pm 0.1) \times 10^{-3}$
8	0.004	$(2 \pm 2) \times 10^{-3}$	0.00781	$(3.94 \pm 0.04) \times 10^{-3}$

Table 8. Astrometry of the reference and second set ($N \sim 10^5$) of reconstructed images using visibility phase information. The "*Reference*" column refer to the synthetic image. The distances are in respect to the brightest star.

Star No.	**Reference Distance** (mas)	**Distance** (mas)
2	7.11	7.13 ± 0.02
3	7.81	7.82 ± 0.02
4	7.6	7.2 ± 0.4
5	8.01	8.04 ± 0.03
6	9.3	9.0 ± 0.3
7	10.3	10.3 ± 0.3
8	12	6 ± 3

Table 9. Photometry of the reference and second set ($N \sim 10^5$) of reconstructed images using visibility phase information. The "*Reference*" column refer to the synthetic image. The flux ratios are in respect to the brightest star.

Star No.	**Reference Flux** (relative)	**Flux** (relative)	**Reference Flux Ratio**	**Flux Ratio**
1	0.501	$(5.02 \pm 0.01) \times 10^{-1}$	–	–
2	0.250	$(2.57 \pm 0.07) \times 10^{-1}$	0.5000	$(5.117 \pm 0.001) \times 10^{-1}$
3	0.125	$(1.28 \pm 0.02) \times 10^{-1}$	0.24999	$(2.5408 \pm 0.0004) \times 10^{-1}$
4	0.06	$(5 \pm 1) \times 10^{-2}$	0.125	$(9.98 \pm 0.02) \times 10^{-2}$
5	0.031	$(2.5 \pm 0.7) \times 10^{-2}$	0.0625	$(4.91 \pm 0.01) \times 10^{-2}$
6	0.016	$(1.1 \pm 0.5) \times 10^{-2}$	0.0312	$(2.11 \pm 0.01) \times 10^{-2}$
7	0.008	$(3 \pm 4) \times 10^{-3}$	0.016	$(6.7 \pm 0.9) \times 10^{-3}$
8	0.004	$(2 \pm 2) \times 10^{-2}$	0.00781	$(4.17 \pm 0.03) \times 10^{-2}$

Table 10. Astrometry of the reference and third set ($N \sim 10^3$) of reconstructed images using closure phase information. The "*Reference*" column refer to the synthetic image. The distances are in respect to the brightest star. Stars 6, 7, and 8 were not detected.

Star No.	**Reference Distance** (mas)	**Distance** (mas)
2	7.11	7.16 ± 0.05
3	7.81	7.86 ± 0.06
4	7.57	7.48 ± 0.09
5	8.0	8.7 ± 0.8

Table 11. Photometry of the reference and third set ($N \sim 10^3$) of reconstructed images using closure phase information. The "*Reference*" column refer to the synthetic image. The flux ratios are in respect to the brightest star. Stars 6, 7, and 8 were not detected.

Star No.	**Reference Flux** (relative)	**Flux** (relative)	**Reference Flux Ratio**	**Flux Ratio**
1	0.501	$(5.04 \pm 0.03) \times 10^{-1}$	–	–
2	0.250	$(2.58 \pm 0.07) \times 10^{-1}$	0.50000	$(5.0336 \pm 0.0003) \times 10^{-1}$
3	0.13	$(1.1 \pm 0.2) \times 10^{-1}$	0.249989	$(2.50713 \pm 0.00007) \times 10^{-1}$
4	0.06	$(4 \pm 2) \times 10^{-2}$	0.12502	$(1.1570 \pm 0.0009) \times 10^{-1}$
5	0.03	$(1 \pm 2) \times 10^{-2}$	0.06249	$(5.661 \pm 0.006) \times 10^{-2}$

Table 12. Astrometry of the reference and third set ($N \sim 10^3$) of reconstructed images using visibility phase information. The "*Reference*" column refer to the synthetic image. The distances are in respect to the brightest star. Stars 7 and 8 were not detected.

Star No.	**Reference Distance** (mas)	**Distance** (mas)
2	7.11	7.13 ± 0.02
3	7.8057	7.8063 ± 0.0006
4	7.57	7.60 ± 0.03
5	8.0	8.3 ± 0.3
6	9.34	9.33 ± 0.02

Table 13. Photometry of the reference and third set ($N \sim 10^3$) of reconstructed images using visibility phase information. The "*Reference*" column refer to the synthetic image. The flux ratios are in respect to the brightest star. Stars 7 and 8 were not detected.

Star No.	**Reference Flux** (relative)	**Flux** (relative)	**Reference Flux Ratio**	**Flux Ratio**
1	0.501	$(4.92 \pm 0.09) \times 10^{-1}$	–	–
2	0.250	$(2.54 \pm 0.04) \times 10^{-1}$	0.5000	$(5.170 \pm 0.002) \times 10^{-1}$
3	0.125	$(1.16 \pm 0.09) \times 10^{-1}$	0.2500	$(2.354 \pm 0.002) \times 10^{-1}$
4	0.063	$(5.6 \pm 0.6) \times 10^{-2}$	0.1250	$(1.142 \pm 0.001) \times 10^{-1}$
5	0.03	$(2 \pm 1) \times 10^{-2}$	0.0625	$(4.18 \pm 0.02) \times 10^{-2}$
6	0.016	$(1.3 \pm 0.3) \times 10^{-2}$	0.03125	$(2.604 \pm 0.005) \times 10^{-2}$